# Utilizing computational thermodynamics in characterization and classification of non-metallic inclusions in Ti-deoxidized steels

**Tuomas Alatarvas*, Henri Tervo**, Antti Kaijalainen**, Qifeng Shu***

** Process Metallurgy Research Unit, Centre for Advanced Steel Research,*

*University of Oulu, P.O. Box 4300, FI-90014 Oulu, Finland*

*** Materials and Mechanical Engineering, Centre for Advanced Steel Research,*

*University of Oulu, P.O. Box 4200, FI-90014 Oulu, Finland*

**Abstract**: Non-metallic inclusions (NMIs) are micrometer-sized particles observed in all steel materials, often considered detrimental. In this study, NMIs in titanium-deoxidized steels were investigated, complemented with thermodynamic assessment for more accurate phase characterization. The NMIs were analyzed with a Jeol JSM-7900F FESEM-EDS (Field Emission Scanning Electron Microscope equipped with Energy Dispersive X-ray Spectroscope). For automated particle analyses on FESEM, Aztec Feature runs were carried out on polished steel samples, providing the elemental composition, in addition to morphological data, for each observed NMI. Utilizing the obtained EDS analyses, the fractions of oxides ($Al_2O_3$, MnO, $TiO_x$), manganese sulfide (MnS), and titanium nitride (TiN) in each NMI are estimated with a MATLAB script. Based on the estimated phase contents, a composition-based classification method for the NMIs is presented. To visualize the phase contents of the observed NMIs, the calculated compositions are plotted on MnO–$TiO_2$–$Ti_2O_3$ ternary diagrams. Computational thermodynamics software FactSage 8.3 was firstly utilized to estimate the fully liquid NMI composition region at steelmaking temperatures in the considered ternary oxide system of MnO–$TiO_2$–$Ti_2O_3$. Secondly, the thermodynamic stability of NMI phases in the steel was assessed with decreasing temperature during the solidification of steel. The current study demonstrates how computational thermodynamics can be utilized in characterization and classification of non-metallic inclusions and giving insight on their formation during solidification of steel.

*Keywords*: computational thermodynamics, non-metallic inclusions, steel

## 1. INTRODUCTION

The composition of non-metallic inclusions (NMIs) in steel is mainly dependent on the total elemental composition of the steel. To enhance steel cleanliness by decreasing the oxygen content, the molten steel must be deoxidized by introducing deoxidation agents. Conventional deoxidation agents include aluminum and silicon, binding the oxygen to $Al_2O_3$ and $SiO_2$ based NMIs. Titanium can be used as a deoxidation agent when titanium oxide based NMIs are desired. These types of NMIs are known to affect the microstructure in welded structures, both in weld metal and in heat-affected zones by inducing the formation of acicular ferrite (Tervo et al. 2020, 2021; Loder et al. 2016)

The titanium contents in Ti-deoxidized steels affect the phases observed in NMIs. According to the presentation by Panda et al. (2019), the MnO–$TiO_2$–$Ti_2O_3$ oxide system includes spinel, ilmenite, and pseudobrookite solid solutions with varying compositions, as illustrated in Fig. 1. According to Wang and Li (2021) and Wang et al. (2018), the higher Mn content in spinel and ilmenite – compared to pseudobrookite – promotes the formation of beneficial acicular ferrite by depleting the Mn content of the steel matrix in the vicinity of NMIs.

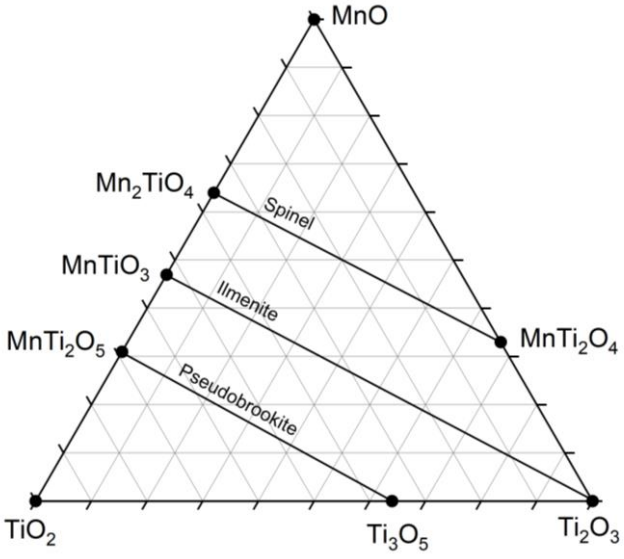


Fig. 1. MnO–$TiO_2$–$Ti_2O_3$ ternary diagram with the main solid solutions.

In addition to the primary NMIs formed during the deoxidation process in the molten steel, other NMIs can form during further processing and solidification of the steel. The primary NMIs can act as nucleation sites for forming phases. To estimate the phases forming in the molten steel and during solidification of steel, thermodynamic assessment can be applied. While the rate of the reactions is not taken into account, the amount and composition of stable phases at a given temperature can be estimated. The assumption of thermodynamic equilibrium can be considered reasonable in molten steel (>1500 °C) with homogeneous composition. As the steel solidifies, kinetics constrain achieving the equilibrium. However, the thermodynamic equilibrium points the direction of possible NMI reactions also in the solid state.

The current study demonstrates how computational thermodynamics and data processing can be utilized in characterization and classification of non-metallic inclusions and giving insight on their formation during solidification of steel.

## 2. MATERIALS AND METHODS

### *2.1 Investigated materials*

In this study, NMIs in two samples of titanium-deoxidized steels were investigated. The materials were denoted as $Ti_{Low}$ and $Ti_{High}$, according to their titanium contents (Tervo et al. 2020, 2021). The chemical compositions of the samples are presented in Table 1. The material was cast in a laboratory to 20 kg ingots. After hot rolling of the ingots, polished cross section samples were prepared for NMI investigation.

Table 1. Composition of the studied steels, in wt%.

| | **$Ti_{Low}$** | **$Ti_{High}$** |
|---|---|---|
| C | 0.05 | 0.05 |
| Si | 0.23 | 0.03 |
| Mn | 1.7 | 1.7 |
| P | 0.007 | 0.005 |
| S | 0.003 | 0.003 |
| Al | 0.003 | 0.002 |
| Nb | 0.01 | 0.01 |
| V | 0.07 | 0.07 |
| Ti | 0.016 | 0.027 |
| N | 0.008 | 0.006 |
| O | 0.0047 | 0.0080 |

### *2.2 Scanning electron microscopy*

Non-metallic inclusions were analyzed with a Jeol JSM-7900F FESEM-EDS (field emission scanning electron microscope with energy dispersive X-ray spectroscopy). The characteristics, including elemental composition and morphology, of particles larger than 2 µm in an equivalent circle diameter were analyzed with *Aztec Feature* automated particle analysis functionality. The scanned section in each sample covered an area of approximately 52 $mm^2$, comprising of total 330 fields at 250x magnification. Figure 2 presents one of the fields imaged with backscattered electron (BSE) detector, illustrating gray NMI particles on light background, i.e., steel.

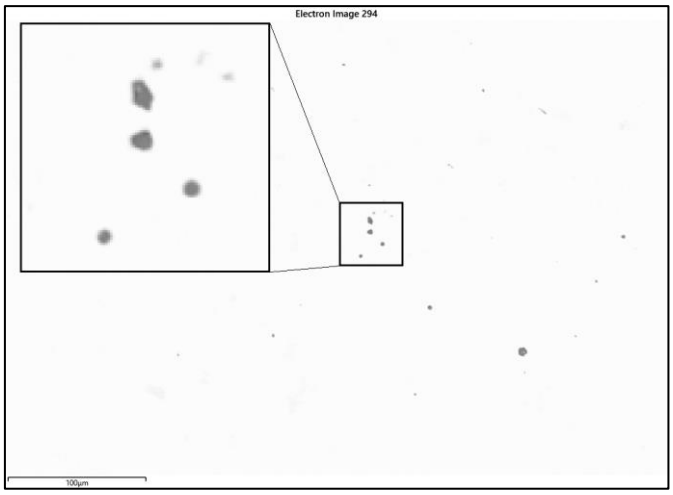


Fig. 2. Single field imaged on FESEM, showing NMI particles in steel.

After the *Feature* runs, representative NMIs were selected from the dataset. High-resolution BSE images and EDS point analyses were acquired after relocating the selected sites.

### *2.3 Classification of non-metallic inclusions*

There are various ways to process the raw data acquired with the *Feature* particle analysis runs (Alatarvas et al 2019, Wartiainen et al. 2020). Here, all particles containing less than 30 wt.% of Al, Mn, N, Ti and S in total were discarded. The remaining particles were considered true NMIs, comprising of components $Al_2O_3$, MnO, MnS, TiN, $TiO_2$ and $Ti_2O_3$. To estimate the phase composition, the following stepwise procedure was applied, utilizing the EDS analyses of Al, Mn, Ti, N, S, and O of each NMI.

1. All analyzed Al bound to $Al_2O_3$,
2. All analyzed S bound to MnS,
3. All analyzed N bound to TiN,
4. Remaining Mn (from the 2nd step) bound to MnO,
5. Remaining Ti (from the 3rd step) and O (from the 1st and 4th step) determine the proportions of $TiO_2$ and $Ti_2O_3$.

The total amount of components was scaled to 100 wt.%, after which the NMIs were classified into combinations of $Al_2O_3$, MnO, MnS, TiN, and $TiO_x$ with a 10 wt.% threshold, totaling 31 combinations, i.e., inclusion classes. For plotting, the oxide system was considered $MnO–TiO_2–Ti_2O_3$, allowing the construction of ternary diagrams.

Executed with MATLAB scripts, the presented approach allows the data processing and visualization of the NMI characteristics in the scanned area, as well as for individual NMIs with point analyses.

### *2.4 Computational thermodynamics*

Computational thermodynamics software FactSage 8.3 (Bale et al. 2002) and its *FToxid* database was used to assess the composition region in the $MnO–TiO_2–Ti_2O_3$ system, where oxides exist only as fully molten slag. Considering steelmaking temperatures (1500–1700 °C) and plotted into ternary $MnO–TiO_2–Ti_2O_3$ diagram with the *Phase Diagram* module, the region is denoted as liquid window. Here, solid

solutions of monoxide, titania spinel, rutile, ilmenite, and pseudobrookite were considered as precipitating phases, included in the considered system.

Further, FactSage was used to assess the stability of NMIs as a function of temperature with the steel compositions reported, with total mass of 100 g of material. *Equilib* module with the databases *FSstel* and *FToxid* were selected for the calculations, with the following solid solutions in addition to liquid steel and liquid slag: FCC (face-centered cubic, austenite), BCC (body-centered cubic, ferrite), cementite ($Fe_3C$), MS-c (MnS–FeS solid solution), A-monoxide, corundum, A-rutile, A-ilmenite, A-olivine, pseudobrookite, B-spinel, and titania spinel were considered. For plotting of the results, also TiN (as FCC phases) was included, known as a possible NMI type, whereas other nitrides and carbides were omitted.

## 3. RESULTS AND DISCUSSION

### *3.1 Sample-specific NMI characteristics*

The *Feature* particle analyses resulted in total of 2623 and 1255 observed particles in $Ti_{Low}$ and $Ti_{High}$ samples, respectively. After applying the compositional criteria, the number of particles were decreased to 2210 and 1177, to represent the true NMIs in $Ti_{Low}$ and $Ti_{High}$ samples, respectively. The results according to the classification procedure are presented in Fig. 3. It can be seen that the number of particles per scanned area is in the range of 22–42 particles per square millimeter. In $Ti_{Low}$ sample, the most dominant NMI class is "MnO MnS TiN $TiO_x$", which translates to oxides in the MnO–TiOx system with precipitated sulfide (MnS) and nitride (TiN) phases. Both samples are also characterized by the occurrence of "MnO TiOx" type inclusions, i.e., oxides without sulfide and nitride phases.

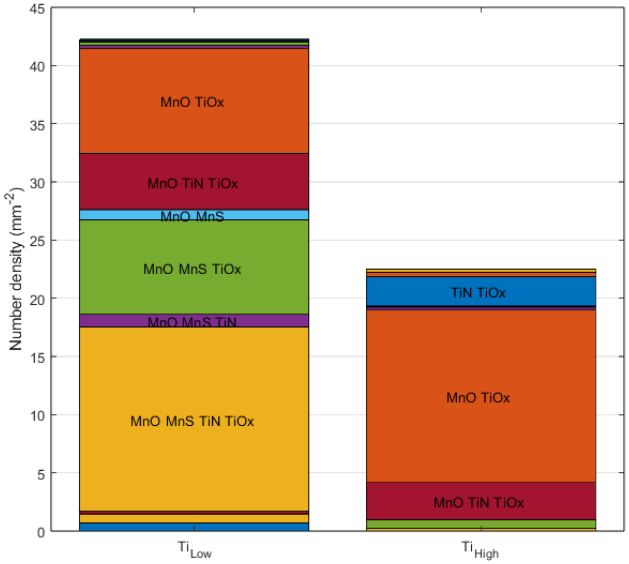


Fig. 3. Number of NMIs per unit area, by NMI classes.

### *3.2 Selected NMIs with point analyses*

Selected NMIs were located from the Feature dataset after the run, saving high-resolution BSE images. The BSE images illustrate compositional contrast: high atomic number (heavy) elements show as brighter areas than low atomic number (light) elements. Therefore, the images can aid in observing the phase complexity of NMIs.

EDS analyses were manually acquired from certain points in the NMIs. Further, the EDS analyses were used as an input in a MATLAB script to visualize the oxide composition in a ternary diagram. In this section, a total of five representative oxide inclusions are presented, with corresponding compositions plotted on ternary diagrams.

In Fig. 4, a BSE image of an oxide NMI in the $Ti_{Low}$ sample is presented. The structure of the NMI comprises of the primary oxide phases (points 8 and 9) with precipitated phases on their surfaces (points 7 and 10). After the calculation procedure and plotting onto ternary diagram, shown in Fig. 5, it is observed that the points 7–9 locate near the pseudobrookite solid solution line ($Mn_2TiO_5$–$Ti_3O_5$). On the other hand, the point 10 is closer to the spinel composition on the $Mn_2TiO_4$– $MnTi_2O_4$ line.

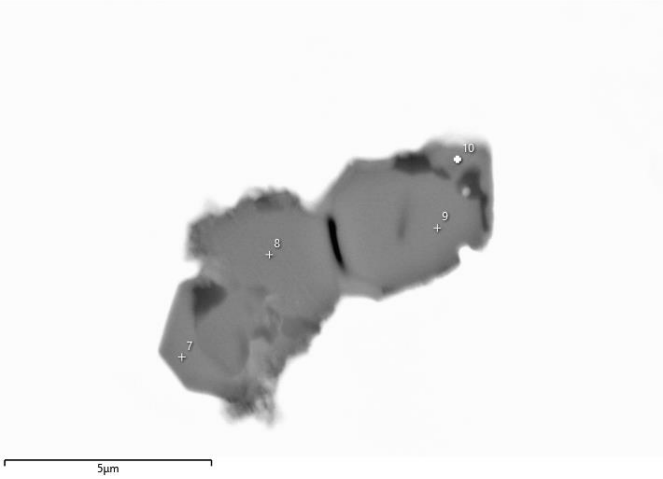


Fig. 4. BSE image of NMI#1, with EDS analyzed points.

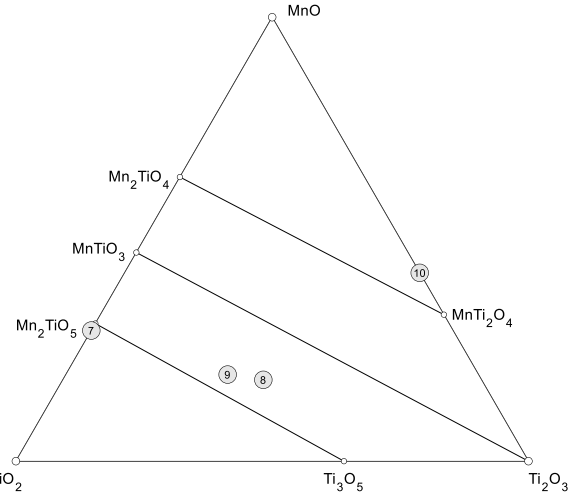


Fig. 5. Estimated oxide compositions of the analyzed points in NMI#1.

Figure 6 presents a BSE image of another oxide NMI in the $Ti_{Low}$ sample. A layered structure is observed, with pseudobrookite phases in the core, found on points 23 and 24, as shown in Fig. 7. The darker phase at point 22 is spinel, according to the phase identification procedure.

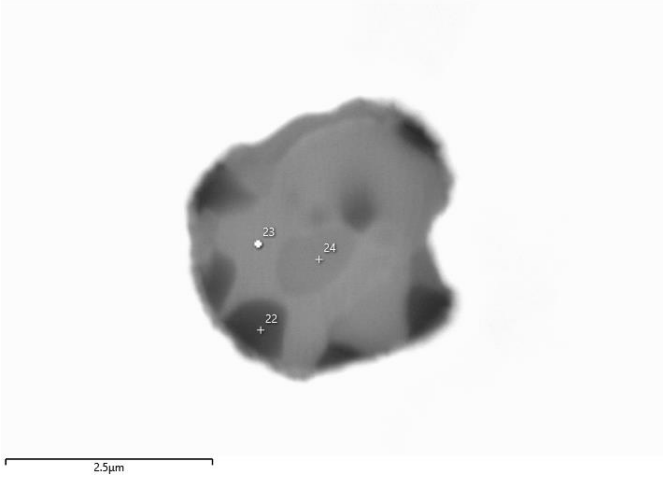


Fig. 6. BSE image of NMI#2, with EDS analyzed points.

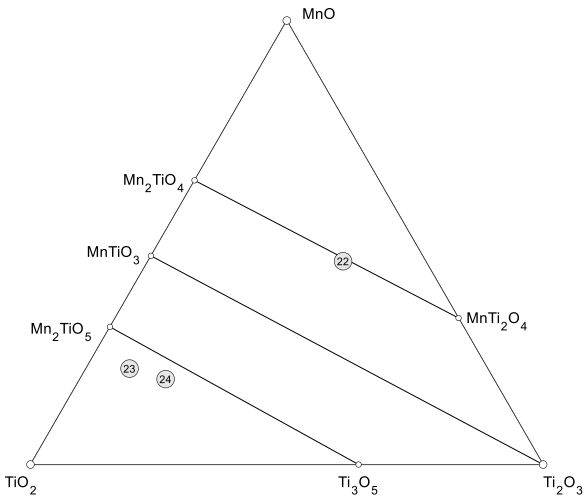


Fig. 7. Estimated oxide compositions of the analyzed points in NMI#2.

A cross section of a spherical NMI is presented in Fig. 8, observed in $Ti_{High}$ sample. The uniform gray shade and the roundness suggest that the NMI has been fully liquid in the molten steel, before solidification. As observed in Fig. 9, the variation in the calculated oxide composition is negligible, with points 1–3 located near the pseudobrookite solid solution line.

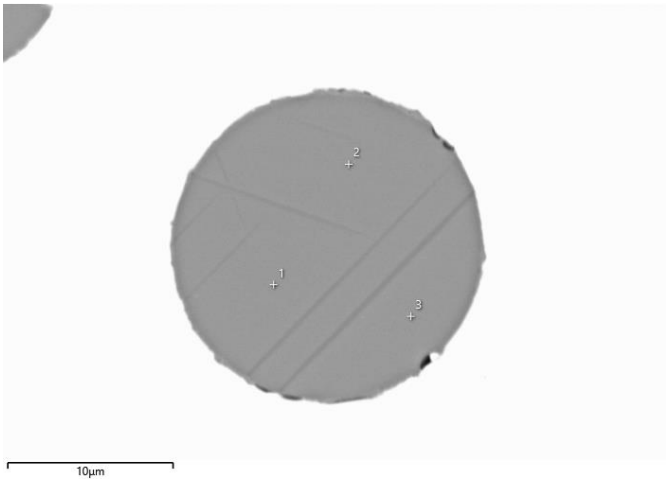


Fig. 8. BSE image of NMI#3, with EDS analyzed points.

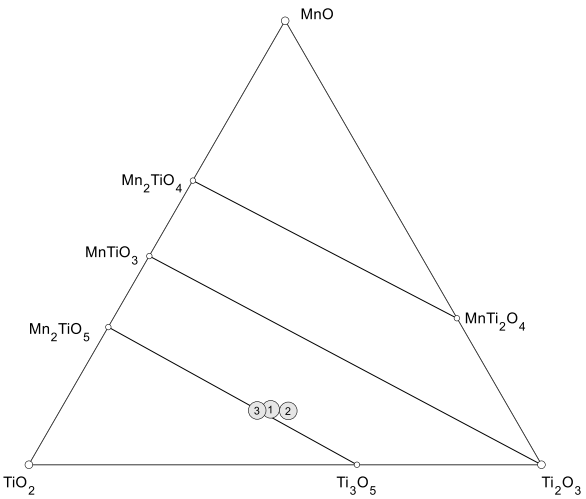


Fig. 9. Estimated oxide compositions of the analyzed points in NMI#3.

In Fig. 10, BSE image of another spherical NMI in the $Ti_{High}$ sample is presented. Comparing with the estimated compositions of points 8–10 in Fig. 11, it is concluded that the main phase is pseudobrookite, which has been most likely molten at steelmaking temperatures. The enclosed light phase has a composition higher in $TiO_2$ content, closer to the rutile corner of the presented ternary diagram.

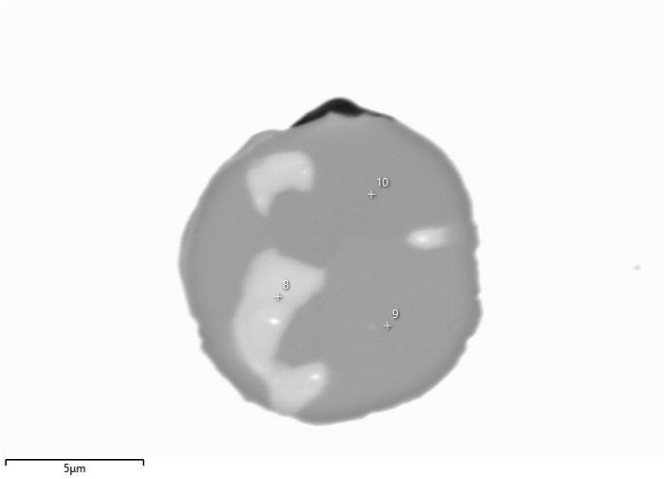


Fig. 10. BSE image of NMI#4, with EDS analyzed points.

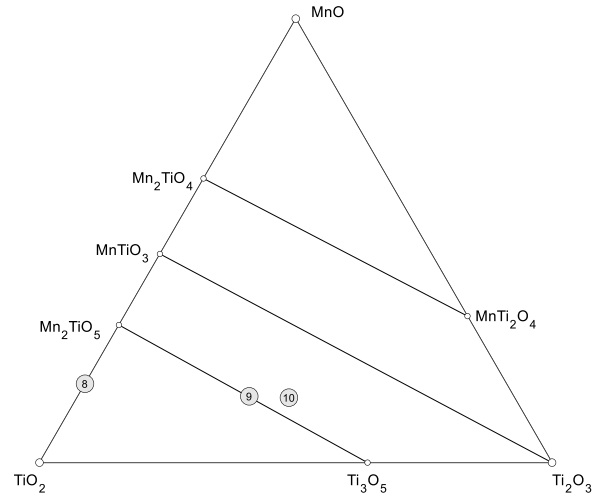


Fig. 11. Estimated oxide compositions of the analyzed points in NMI#4.

Some agglomerated NMIs were observed in the $Ti_{High}$ sample. The NMI presented in Fig. 12 is separated by a crack, seen as a black stripe in the BSE image. The primary composition of the oxides (points 16–19) are located near the pseudobrookite line. The composition of point 20 is nearly all titanium nitride (TiN), thus it is not plotted in the oxide ternary diagram in Fig. 13. Found on the periphery of the NMI, it can be concluded TiN has precipitated as a secondary phase on the surface of the primary oxide NMI during the solidification of the steel.

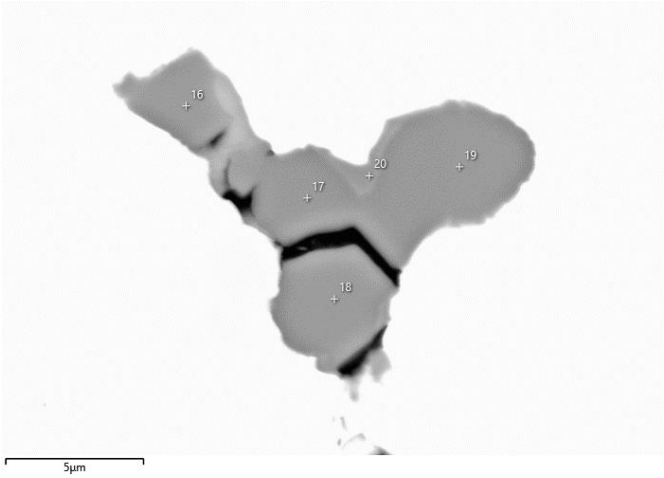


Fig. 12. BSE image of NMI#5, with EDS analyzed points.

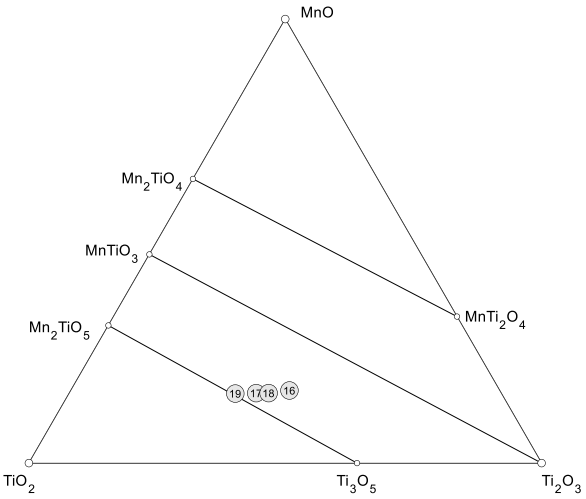


Fig. 13. Estimated oxide compositions of the analyzed points in NMI#5.

### *3.3 Liquid window in the MnO–$TiO_2$–$Ti_2O_3$ system*

Figure 14 presents the colored-line isotherms 1500 °C, 1600 °C, and 1700 °C for all-liquid regions in the MnO–$TiO_2$–$Ti_2O_3$ oxide system. At 1500 °C, the liquid window is located between the MnO and $TiO_2$ compositions, extending slightly towards the $Ti_2O_3$ corner. Increasing the temperature to 1600 °C and 1700 °C, the all-liquid region expands notably. The univariant phase regions, separated by black lines, show the first-precipitating phases when an all-liquid slag with a certain composition starts to solidify. The chemical composition of the presented spherical NMIs corresponds to pseudobrookite phase, fully molten at 1600 °C.

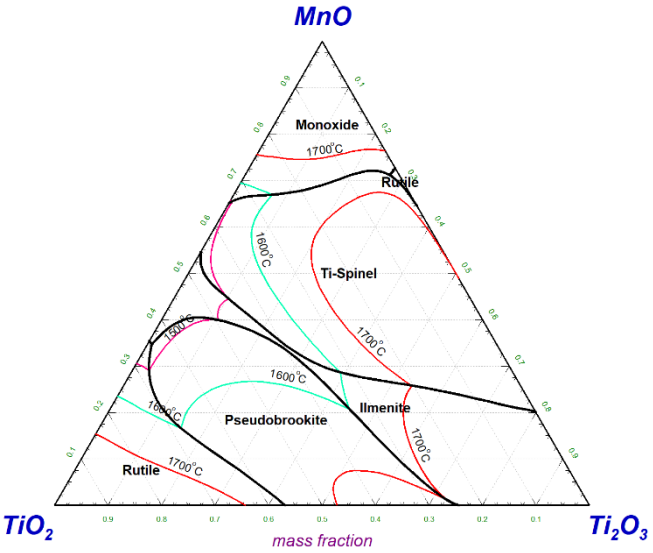


Fig. 14. All-liquid isotherms and univariant phases in the MnO–$TiO_2$–$Ti_2O_3$ oxide system.

### *3.4 Thermodynamic stability of NMIs*

Figures 15 and 16 present the mass of thermodynamically stable phases as a function of decreasing temperature, depicting the solidification of steel. As the total mass of the system is constant 100 g, the mass corresponds to weight percentages in the system. The results show some similarities because of the comparable steel compositions. The slight variations originate from the differences in aluminum, titanium, oxygen, and nitrogen contents.

For both samples, all NMIs are as fully liquid slag until around 1650 °C. Excluding steel, the first solid solution to precipitate is pseudobrookite in both cases. As the solidification of steel progresses, titanium nitride TiN and manganese sulfide MnS start to form as well. As the temperature further decreases, a transformation of oxides can be observed: first pseudobrookite to corundum and ilmenite, then towards spinel and olivine stability. In practice, kinetics constrain the reactions in the solid state, thus the equilibrium at lower temperatures is never achieved. Comparing the calculations to the observed NMI#2 presented in Fig. 6, the results are in line. The core of the NMI is pseudobrookite, since it is the first precipitating solid phase from the fully liquid oxide inclusions. On the periphery of pseudobrookite, spinel phases are observed, further precipitated during solidification.

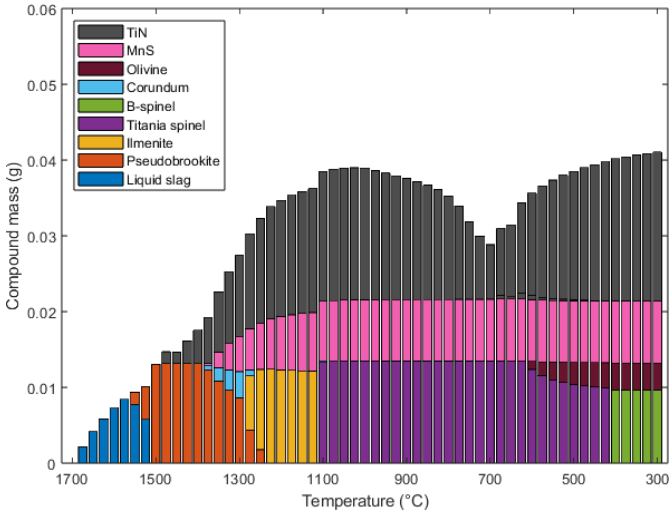


Fig. 15. Mass of stable compounds in $Ti_{Low}$ sample.

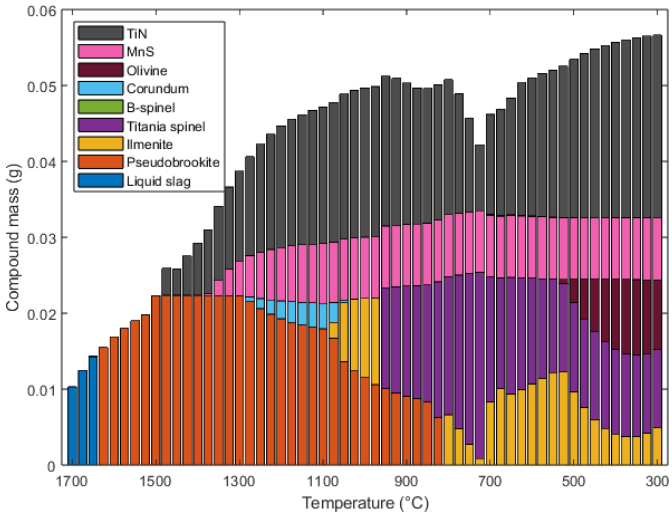


Fig. 16. Mass of stable compounds in $Ti_{High}$ sample.

## 4. CONCLUSIONS

A case study of classification and characterization of NMIs in titanium-deoxidized steel samples is presented. The analysis is coupled with computational thermodynamics. Data processing and visualization was executed by MATLAB scripts to automate the procedures. The presented approach allows the data processing and visualization of the total NMI characteristics in the scanned area, as well as for individual NMIs.

Utilizing the presented methods, the sample-specific NMI types were presented, and for individual NMIs, oxide phases in the MnO–$TiO_2$–$Ti_2O_3$ system were identified. The primary oxide phases were pseudobrookite, a finding supported by the thermodynamic calculations. The spherical shape and homogeneous composition of pseudobrookite NMIs suggest they have been completely liquid in the molten steel. Spinel and TiN phases were observed as precipitated phases on the surface of pseudobrookite NMIs.

DOI: 10.3384/ecp212.025

ACKNOWLEDGEMENTS

This research is a part of the CLEAN2STEEL project that benefits from the financial and strategic support of the Kvantum Institute, University of Oulu. H.T. and A.K. are grateful to the funding of the research program FOSSA II (Fossil-Free Steel Applications: Phase II, Dnro 5562/31/2023) funded by Business Finland. SSAB Europe Oy is acknowledged for the provision of the studied materials.

REFERENCES

Alatarvas T., Antola, T., and Fabritius, T. (2019). Utilizing inclusion data in characterization of oxide-sulfide stringers in hot-rolled plates. *IOP Conference Series: Materials Science and Engineering*, 529(1), 012066.

Bale, C.W., Chartrand, P., Degterov, S.A., Eriksson, G., Hack, K., Mahfoud, R.B., Melançon, J., Pelton, A.D., and Petersen, S. (2002). FactSage Thermochemical Software and Databases. *Calphad* 26(2), 189–228.

Loder, D., Michelic, S.K., and Bernhard, C., (2016). Acicular ferrite formation and its influencing factors - a review. *Journal of Materials Science Research,* 6(1) 24–43.

Panda, S.K., Hudon, P., and Jung I.-H. (2019). Coupled experimental study and thermodynamic modeling of the $MnO$-$Mn_2O_3$-$Ti_2O_3$-$TiO_2$ system. *Calphad*, 66, 101639.

Tervo, H., Kaijalainen, A., Javaheri, V., Kolli, S., Alatarvas, T., Anttila, S., and Kömi, J. (2020). Characterization of Coarse-Grained Heat-Affected Zones in Al and Ti-Deoxidized Offshore Steels. *Metals*, 10, 1096.

Tervo, H., Kaijalainen, A., Javaheri, V., Ali, M., Alatarvas, T., Mehtonen, M., Anttila, S., and Kömi, J. (2021). Comparison of Impact Toughness in Simulated Coarse-Grained Heat-Affected Zone of Al-Deoxidized and Ti-Deoxidized Offshore Steels. *Metals*, 11, 1783.

Wang, B. and Li, J. (2021) Effect of Mn Content on the Characteristics of Inclusions in Ti-Containing Steel Welds. *Metals and Materials International,* 27(8), 2656–2665.

Wang, B., Liu, X., and Wang G. (2018). Inclusion Characteristics and Acicular Ferrite Nucleation in Ti-Containing Weld Metals of X80 Pipeline Steel. *Metallurgical and Materials Transactions B*, 49(6), 2124–2138.

Wartiainen A.-M., Harju, M., Tamminen, S., Määttä, L., Alatarvas, T., and Röning, J. (2020). A tool for finding inclusion clusters in steel SEM specimens. *Open Engineering,* 10(1), 642–648.